HHS Public Access

Author manuscript

Adv Biol Regul. Author manuscript; available in PMC 2023 January 01.

Published in final edited form as:

Adv Biol Regul. 2022 January ; 83: 100858. doi:10.1016/j.jbior.2021.100858.

Bisphosphate nucleotidase 2 (BPNT2), a molecular target of lithium, regulates chondroitin sulfation patterns in the cerebral cortex and hippocampus

BS Eisele[1,2], **AJ Wu**[2], **Z Luka**[2], **AT Hale**[2], **JD York**[2,*]

[1]Department of Pharmacology, Vanderbilt University, Nashville, TN, USA.

[2]Department of Biochemistry, Vanderbilt University, Nashville, TN, USA.

Abstract

Bisphosphate nucleotidase 2 (BPNT2) is a member of a family of phosphatases that are directly inhibited by lithium, the first-line medication for bipolar disorder. BPNT2 is localized to the Golgi, where it metabolizes the by-products of glycosaminoglycan sulfation reactions. BPNT2-knockout mice exhibit impairments in total-body chondroitin-4-sulfation which lead to abnormal skeletal development (chondrodysplasia). These mice die in the perinatal period, which has previously prevented the investigation of BPNT2 in the adult nervous system. Previous work has demonstrated the importance of chondroitin sulfation in the brain, as chondroitin-4-sulfate is a major component of perineuronal nets (PNNs), a specialized neuronal extracellular matrix which mediates synaptic plasticity and regulates certain behaviors. We hypothesized that the loss of BPNT2 in the nervous system would decrease chondroitin-4-sulfation and PNNs in the brain, which would coincide with behavioral abnormalities. We used Cre-lox breeding to knockout *Bpnt2* specifically in the nervous system using *Bpnt2* floxed (fl/fl) animals and a Nestin-driven Cre recombinase. These mice are viable into adulthood, and do not display gross physical abnormalities. We identified decreases in total glycosaminoglycan sulfation across selected brain regions, and specifically show decreases in chondroitin-4-sulfation which correspond with increases in chondroitin-6-sulfation. Interestingly, these changes were not correlated with gross alterations in PNNs. We also subjected these mice to a selection of neurobehavioral assessments and did not identify significant behavioral abnormalities. In summary, this work demonstrates that BPNT2, a known target of lithium, is important for glycosaminoglycan sulfation in the brain, suggesting that lithium-mediated inhibition of BPNT2 in the nervous system warrants further investigation.

*Correspondence to: John D. York. john.york@vanderbilt.edu.

Author Contributions: B.S.E. and J.D.Y. conceived of the experiments and wrote the manuscript. B.S.E. designed and performed the majority of the experiments described herein, Z.L. performed HPLC analyses, A.J.W. and A.T.H. established and maintained the mouse colony and A.J.W performed mouse behavioral experiments.

Keywords

bisphosphate nucleotidase 2; chondroitin sulfate; extracellular matrix; glycosaminoglycan; Golgi; perineuronal net

Introduction

Bisphosphate nucleotidase enzymes metabolize the by-products of intracellular sulfation reactions (Hudson and York 2012). These enzymes are also inhibitory targets of lithium, the first-line pharmacologic agent for bipolar disorder (Benard et al. 2016). Despite an unclear mechanism of action and a vast side effect profile, lithium is an important therapeutic agent that is continually being investigated as a treatment for an array of psychiatric and neurologic disorders (Yang et al. 2012; Saccà et al. 2015; Karimi et al. 2017; Forlenza, De-Paula, and Diniz 2014). Understanding the biochemical consequences of lithium treatment on the bisphosphate nucleotidases therefore could shed light on the pharmacologic mechanisms or toxic effects of lithium.

Bisphosphate nucleotidase 2 (BPNT2, previously known as IMPAD1 (Nizon et al. 2012), JAWS (Sohaskey et al. 2008), GPAPP (Frederick et al. 2008)) is a Golgi-resident nucleotidase (Frederick et al. 2008). BPNT2 acts downstream of Golgi-localized sulfotransferases, which utilize the sulfate group from phosphoadenosine phosphosulfate (PAPS) to yield sulfated products and the by-product phosphoadenosine phosphate (PAP). BPNT2 then catalyzes the breakdown of PAP to adenosine monophosphate (AMP) (Frederick et al. 2008). Golgi-sulfotransferases are primarily carbohydrate sulfotransferases which sulfate glycosaminoglycans (Fukuda et al. n.d.). Loss of BPNT2 disrupts sulfation of glycosaminoglycans (GAGs), especially chondroitin-4-sulfate (Frederick et al. 2008), which is a major component of cartilage. *Bpnt2*-knockout mice exhibit a chondrodysplastic phenotype, characterized by shortened long bones and joint abnormalities (Frederick et al. 2008; Mitchell et al. 2001; Sohaskey et al. 2008) due to impaired bone and cartilage development. These mice die in the perinatal period, likely due to pulmonary insufficiency secondary to an underdeveloped ribcage. Notable, an autosomal recessive human chondrodysplasia caused by mutations in *BPNT2* has also been identified (Nizon et al. 2012; Vissers et al. 2011), implicating BPNT2 as an important regulator of chondrogenesis in humans.

We recently reported that the defects in sulfation seen with *Bpnt2*-knockout stem from a loss of the catalytic activity of the enzyme, and that human disease-associated mutations are located in close proximity to the catalytic motif(Eisele et al. 2021b). We also demonstrated that lithium impairs sulfation *in vitro* in a BPNT2-dependent fashion (Eisele et al. 2021). Given lithium's relevance in the treatment of neuropsychiatric disease, we wanted to investigate whether the loss of BPNT2 in the nervous system could elicit alterations in brain chemistry or behavior.

There is substantial evidence suggesting chondroitin-sulfate is involved in neuronal function (Miyata and Kitagawa 2016b; Sorg et al. 2016). Multiple populations of neurons are surrounded by a specialized extracellular matrix known as the perineuronal network: an

emerging interest for many neuroscientists (Lasek, Chen, and Chen 2017; Berretta et al. 2015; Dzyubenko, Gottschling, and Faissner 2016; van 't Spijker and Kwok 2017; Donegan and Lodge 2016). Perineuronal nets (PNNs) consist primarily of condensed chondroitin sulfate, with chondroitin-4-sulfate being the major species in the adult brain and chondroitin-6-sulfate comprising the minority (Miyata and Kitagawa 2016a). PNNs are generally seen as barriers to neuroplasticity (Harry Pantazopoulos and Berretta 2016), and may be involved in stabilization of neural circuitry (such as that underlying long-term memories (Thompson et al. 2018; Gogolla et al. 2009) and addiction (Lasek, Chen, and Chen 2017)). Throughout postnatal development, plasticity tends to decrease; this correlates with an increase in PNN density over time (Ueno et al. 2018; Brückner and Grosche 2001; Mauney et al. 2013; Miyata and Kitagawa 2016b). Given the "restrictive" nature of PNNs, they are also believed to negatively regulate neurite outgrowth and axon extension. Classically, PNNs surround inhibitory interneurons (Baker, Gray, and Richardson 2017), and they are thus thought to regulate the balance between excitatory and inhibitory signaling in the brain—a balance which is disrupted in acute mania and psychosis (Harry Pantazopoulos and Berretta 2016; Benes and Berretta 2001). Interestingly, alterations in perineuronal nets have been reported in psychiatric diseases (Harry Pantazopoulos and Berretta 2016; Harry Pantazopoulos et al. 2010; Berretta et al. 2015), including schizophrenia (Mauney et al. 2013) and bipolar disorder (H. Pantazopoulos et al. 2015).

Previous work has shown that disrupting the formation of chondroitin alters PNN morphology and rodent behavioral characteristics, including performance on tasks of motor coordination, activity, startle response, and object recognition memory (Yoshioka et al. 2017; Rowlands et al. 2018; Romberg et al. 2013). These traits coincided with decreases in PNNs throughout the brain, as identified by immunohistochemistry (Yoshioka et al. 2017; Rowlands et al. 2018; Romberg et al. 2013).

Given BPNT2's role in chondroitin sulfation, we hypothesized that BPNT2 is important for the sulfation of GAGs (especially chondroitin-4-sulfate) in the brain, and for the development of PNNs and PNN-associated behaviors. Because of the perinatal lethality of the conventional *Bpnt2*-knockout mouse, we have previously been unable to study BPNT2 in the adult mouse brain. In this work, we generated a nervous system-specific *Bpnt2*-knockout mouse ($Bpnt2^{fl/fl}$ Nestin-Cre), which is viable and does not display gross physical abnormalities. We then analyzed GAG sulfation patterns, including the chondroitin sulfation profile. We utilized the common histological PNN marker, *Wisteria floribunda* agglutinin (WFA) to analyze PNN histology, and subjected experimental animals to a selection of neurobehavioral assays which are associated with PNNs.

Materials and Methods

Animals.

All animal experiments were carried out in compliance with the Vanderbilt University Institutional Animal Care and Use Committee (IACUC). Mice were housed on a 12hr light/dark cycle. All assessments were conducted during the light phase. The originating mouse strain used for this research project, C57BL/6N-Bpnt2tm1a(KOMP)Wtsi/Mmucd, RRID:MMRRC_048210-UCD, was obtained from the Mutant Mouse Resource and

Research Center (MMRRC) at University of California at Davis, an NIH-funded strain repository, and was donated to the MMRRC by The KOMP Repository, University of California, Davis; Originating from Ramiro Ramirez-Solis, CSD. Tm1a (targeted allele) animals were bred with mice expressing FLP recombinase (Jackson Labs, #011065) to generate *Bpnt2*-floxed (tm1c, conditional allele) mice. Floxed mice were bred with mice expressing Cre recombinase under the Nestin promoter (Jackson Labs, #003771) to knock out *Bpnt2* (producing the tm1d null allele) in the nervous system (neurons and astrocytes). Mice were identified by ear-tagging and tail DNA was used for genotyping. Genotyping primers to detect *Bpnt2* alleles were: F: 5'-TTAGAAAGGTCCCAGGTTGGCTTCC-3' and R: 5'-AAGCTCTGGTACATGCCTACCATCC-3'. For wild-type allele, the primers yielded a 684 bp product, and for conditional allele, primers yielded a 786 bp product. Nestin-Cre genotyping was performed with primer sequences available from Jackson Labs. Nestin-Cre was kept heterozygous in all mice used for breeding and experiments. All mice used for endpoint experiments were of mixed C57BL/6N and C57BL/6J background. Both male and female mice were used; sex differences were not detected in molecular or behavioral results. All analyses were run on adult mice between 12 and 18 weeks of age.

Quantitative PCR.

Mice were sacrificed by decapitation. Brains were extracted and one hemisphere was immediately dissected and tissues were flash frozen on dry ice. RNA was extracted using Qiagen RNeasy Mini Kit using Qiagen DNase I. cDNA was synthesized from 1 ug of RNA using iScript cDNA synthesis kit (Bio-Rad). PCR reaction was carried out using SsoAdvanced Universal SYBR Green Supermix (Bio-Rad) according to manufacturer instructions. *Bpnt2* mRNA expression (F: 5'-CGCCGATGATAAGATGACCAG-3' and R: 5'-GCATCCACATGTTCCTCAGTA-3') was normalized to *Hprt* mRNA expression (F: 5'-GCAGTACAGCCCCAAAATGG-3' and R: 5'- ATCCAACAAAGTCTGGCCTGT-3') to determine relative transcript enrichment.

Immunoblotting.

Protein was collected from cells lysed in RIPA buffer with protease inhibitor (Roche). Protein extracts were quantified using BCA assay and passed through a 25g needle to break up DNA. 10 ug of total protein was loaded per lane onto a 12% SDS-PAGE gel (Bio-Rad), which was run at 100 V for 90 minutes. Proteins were transferred to a 0.2 um PVDF membrane (Bio-Rad) using TransblotTurbo (Bio-Rad) at 1.3A for 7 minutes. Blots were incubated in primary antibodies (sheep anti-BPNT2, 1:1000, Invitrogen #PA5-47893; mouse anti-Actin, 1:1000, Invitrogen #MA1-744) overnight at 4C, washed 3 times in 0.1% TBS-Tween then in secondary antibodies (AlexaFluor680 anti-sheep 1:20,000; AlexaFluor800 anti-mouse 1:20,000) for 2 hours at room temperature and washed 3 times in 0.1% TBS-T. Blots were imaged on LiCor Odyssey and analyzed using ImageJ.

Glycosaminoglycan analysis.

Flash-frozen brain regions (10–15 mg of tissue) were homogenized in 400 ul GAG preparation buffer (50 mM Tris, pH 8.0, 10 mM NaCl, 3 mM $MgCl_2$) using tissue pestle. 50 ul of homogenate was taken and centrifuged at 12000rpm, and supernatant was used to determine soluble protein content using Pierce BCA assay. 4 ul of Proteinase K (2

mg/ml) was added to the remaining homogenate, and sample was incubated overnight at 56C. After digest, the samples were heated at 90C for 30 minutes to denature Proteinase K. Precipitated material was separated by centrifugation. Dimethylmethylene blue (DMMB) assay. An aliquot of supernatant was used for DMMB analysis of total sulfated GAGs. 20 ul of each sample was added to a 96-well clear-bottomed microplate in duplicate. 200 ul of pH 1.5 DMMB reagent (prepared according to Zheng and Levenston(Zheng and Levenston 2015)) was added to each well using a multichannel pipette. Absorption was immediately measured at 525 and 595 nm, and 595 measurement was subtracted from 525 measurement to yield final reading. Quantity of sulfated GAG was determined by comparison to a standard curve of bovine chondroitin-4-sulfate (Sigma) prepared in GAG preparation buffer. Amounts of sulfated GAG were normalized to protein concentration. High-performance liquid chromatography (HPLC). Sample buffer was changed to 0.1 M ammonium acetate, pH 7.0 by using 3 kDa Millipore concentrator by concentration/dilution until initial concentration of homogenization buffer decreased 500-times. The volume of concentrated samples was adjusted to 70 ul and 3 ul of Chondroitinase ABC (1.4 U/ml Stock solution, containing BSA, SEIKAGAKU) was added to each sample. Reaction mixture was incubated at 37C for 4 hours. After chondroitinase ABC cleavage, 130 ul of water was added. Released disaccharides were filtered through a 10 kDa concentrator. This procedure was repeated once more to improve yield. GAG samples were lyophilized using a SpeedVac at 25 °C overnight. Lyophilized samples were stored at −80C until fluorescent labeling. *2-AB derivatization*. Labeling of disaccharides was performed with 2-aminobenzamide (2-AB) by published procedure (4). An aliquot of 5–7 ul of labeling mixture (0.35 M 2-AB, 1 M $NaCNBH_3$ solution in 30% acetic acid in dimethyl sulfoxide) was added to lyophilized samples or disaccharide standards and the mixture was incubated for 3 hours at 65C. Labeling reaction mixtures were spotted on a strip of Whatman 3MChr paper and washed with 1 ml of acetonitrile six times. Cleaned disaccharides were eluted with three aliquots of 50, 75 and 75 ul of water by using 0.2 um centrifugal device. *HPLC.* The analysis of labeled disaccharides was performed by HPLC. The HPLC system included Waters 515 Pumps, Waters 517plus Autosampler, Waters Pump Control Module II and Shimadzu RF-10Axl spectrofluorometer detector under Waters Empower software. Samples analysis performed on Supelco-LC-NH_2 25 cm × 4.6 mm (Sigma). Column was equilibrated with 16 mM NaH_2PO_4 with flow rate of 1 ml/min. The samples of 50–100 ul were injected and eluted with 60 min linear gradient 16 mM – 800 mM NaH_2PO_4 with flow rate of 1 ml/min as in (5). Disaccharide elution was monitored by fluorescence at 420 nm with excitation at 330 nm. Peak identities were determined by running Δdi-0S, Δdi-6S, and Δdi-4S standards (Sigma) prior to running samples. Chromatograms were analyzed by Empower software.

Immunofluorescence.

Mice were sacrificed by decapitation. Brains were extracted and one hemisphere was flash frozen in OCT compound then sectioned into 30-um-thick slices on a Leica cryostat at −20C. Tissue slices were fixed in 4% paraformaldehyde for 15 minutes then rinsed twice in 1X PBS containing 0.3% Triton X-100 (PBS-T), 10 minutes per wash. Slides were blocked in blocking buffer (PBS-T containing 10% goat serum) for 30 minutes at room temperature, then covered in primary antibody (WFA-biotin conjugate, 1:500, Sigma #L1516) in blocking buffer diluted 1:3 in PBS-T and incubated for 1.5 hours at room temperature. Slides

were then washed in diluted blocking buffer 3 × 5 minutes, then covered in secondary antibody (Streptavidin-AlexaFluor488, 1:500) in diluted blocking buffer for 1 hour at room temperature in a humidified container, protected from light. Slides were washed in diluted blocking buffer 3 × 5 minutes. Coverslips were affixed to slides using ProLong™ Gold Antifade Mountant with DAPI (Life Technologies) and allowed to dry overnight before imaging the following day. Images were taken at 4X and 20X magnification on a Nikon Eclipse Ti inverted fluorescent microscope. 20X images were taken in z-stacks of 25 images, 0.4 um apart. Summed-stack images were used for PNN analysis using commercially available PipsqueakAI software (Rewire Neuro). PNNs from approximately 8 fields of view from each of 2 slices of tissue (per region analyzed) were measured from each animal (3–7 animals per genotype). PNN fluorescence measurements from each animal were averaged, and individual animal averages were used for statistical calculations between genotypes(Lord et al. 2020).

In vivo behavior (in order of testing).

Elevated zero maze. Mice were placed individually on the open arm of an elevated zero maze (Med Associates) and behavior was tracked using AnyMaze software for 5 minutes. Open field activity analysis. Open-field behavior was examined for 45 min using the infrared photobeam Med Associates system for mice. Novel object recognition. Mice were habituated to a Y-maze for 2 days (5 minutes per day). On training day, 2 identical objects were placed in each of the 2 non-starting arms of the maze, and the mouse was allowed to explore objects for 5 minutes. On testing day, one of the two objects was replaced with a novel object, and the mouse was allowed to explore objects for 5 minutes. The 5 minute training and testing phases were recorded using AnyMaze software, and time spent interacting with objects was measured by 2 independent scorers, blinded to mouse genotype. Scores were averaged, and averages were used to determine discrimination ratios. Accelerating rotarod. Mice were placed on a cylinder (~3 cm in diameter) which initially rotates at 4 rpm and accelerates to 40 rpm. The latency to falling off the rotarod was measured as an index of motor coordination (maximum trial length of 300 seconds). Trials were repeated 3 times daily, over a course of 3 days. Tail suspension. Mouse tails were taped to a vertical aluminum bar connected to a strain gauge inside a commercial tail suspension test chamber (Med Associates). Motion was recorded over 6 minutes. Startle/ Prepulse inhibition. The startle response to 40-ms 120-dB white noise and its inhibition by a prepulse was examined using the Acoustic Startle Reflex Package for mice from Med Associates. Mice were placed in a clear plastic cylinder (~5 cm diam) within a ventilated sound-attenuating enclosure, and given 5 minutes to acclimate. Startle stimulus was presented in the presence or absence of a 20-ms prepulse presented at 70, 76, 82, or 88 dB, 100-ms before the stimulus. The maximal startle amplitude recorded during a 65-msec sampling window after stimulus presentation was used as the dependent variable. Stimuli were presented in a total of 54 trials, and startle response or prepulse inhibition were averaged across trials.

Results

Generation of a nervous system-specific Bpnt2-knockout mouse.

An illustration of the knockout strategy is shown in Figure 1A. The second exon of the *Bpnt2* gene was flanked by loxp sites, generating a “floxed” (fl) allele. When bred with a Nestin-Cre mouse, the second exon was excised, preventing functional protein expression in nervous system tissues. A section of cerebral cortex was used to confirm near-absence of *Bpnt2* mRNA expression (Figure 1B) and BPNT2 protein expression (Figures 1C, 1D) in *Bpnt2*$^{fl/fl}$ Nestin-Cre mice relative to *Bpnt2*$^{fl/fl}$ and heterozygous *Bpnt2*$^{fl/+}$ Nestin-Cre controls. *Bpnt2*$^{fl/fl}$ Nestin-Cre animals were viable and did not display gross physical abnormalities.

Glycosaminoglycan sulfation in brain tissue from Bpnt2$^{fl/fl}$ Nestin-Cre mice is impaired.

We next investigated whether overall GAG sulfation was altered in the brains of *Bpnt2*$^{fl/fl}$ Nestin-Cre mice. We analyzed total GAG sulfation in two brain regions associated with perineuronal nets: visual cortex(Pizzorusso et al. 2002) and hippocampus(Harry Pantazopoulos et al. 2010). Total sulfated GAG was measured in tissue homogenates using dimethylmethylene blue assay(Farndale, Buttle, and Barrett 1986), and sulfated GAG content was normalized to total protein concentration. As predicted, *Bpnt2*$^{fl/fl}$ Nestin-Cre mice exhibited decreased sulfated GAG (normalized to total protein content) in both visual cortex and hippocampus relative to Nestin-Cre-only, *Bpnt2*$^{fl/fl}$, and *Bpnt2*$^{fl/+}$ Nestin-Cre controls (Figures 2A, 2B).

Chondroitin sulfation patterns are altered in brain tissue from Bpnt2$^{fl/fl}$ Nestin-Cre mice.

To more specifically analyze sulfated moieties, we next sought to analyze alterations in chondroitin sulfation patterns in the visual cortex and the hippocampus. Because we did not identify alterations in overall sulfation among the three control groups (Nestin-Cre-only, *Bpnt2*$^{fl/fl}$, and *Bpnt2*$^{fl/+}$ +Nestin-Cre), we elected to analyze only *Bpnt2*$^{fl/fl}$ and *Bpnt2*$^{fl/fl}$ Nestin-Cre brain tissues. Following digestion of samples with chondroitinase ABC, chondroitin disaccharides were fluorescently labeled and resolved by high-performance liquid chromatography (HPLC). We measured ratios of each of the major species of chondroitin (0S, 4S, and 6S) to the total peak area of all three species. Using this approach, we identified clear and statistically signficant decreases in 4S disaccharide (Δdi-4S), which corresponded with a significant increase in unsulfated disaccharide (Δdi-0S). These findings recapitulate those seen in the cartilage extracts from germline *Bpnt2*-knockout mice(Frederick et al. 2008). Interestingly, we also observed an *increase* in 6S disaccharide (Δdi-6S), which was not previously observed in tissues from the germline *Bpnt2*-knockout mouse. Results from visual cortex are shown in Figure 2C, and results from hippocampus are shown in Figure 2D. Representative HPLC traces from visual cortex samples are shown in Figures 2E, 2F.

Perineuronal nets (as measured by WFA staining) are not grossly altered in Bpnt2$^{fl/fl}$ Nestin-Cre mice.

Other groups have examined genetic manipulations that affect the development of chondroitin sulfate proteoglycans in the brain and have identified alterations in perineuronal nets(Yoshioka et al. 2017; Rowlands et al. 2018), as measured by conventional histological methods (namely, WFA staining). We therefore decided to evaluate perineuronal net staining in cortical and hippocampal regions of *Bpnt2*$^{fl/fl}$ Nestin-Cre mouse brain relative to *Bpnt2*$^{fl/fl}$ controls. Tissues sections were stained with WFA and then analyzed using commercially available PipsqueakAI software, which automatically detects perineuronal nets and reports fluorescence intensity relative to background staining(Slaker, Harkness, and Sorg 2016). We did not observe gross alterations in WFA fluorescence (Figure 3A), nor did we observe significant alterations in PNN staining measurements in cortical (Figure 3B) or hippocampal (Figure 3C) regions. As a secondary measure, we also analyzed the number of PNNs detected by PipsqueakAI per field of view in both cortical (Figure 3D) and hippocampal regions (Figure 3E), and we did not observe significant differences in number of PNNs.

Bpnt2$^{fl/fl}$ Nestin-Cre mice do not exhibit alterations in behavior across a selection of behavioral tests.

As a final analysis of the consequences of loss of BPNT2 in the nervous system, we subjected mice to a series of neurobehavioral experiments, which have been previously associated with alterations in PNNs, including open-field activity analysis(Yoshioka et al. 2017), novel object recognition(Rowlands et al. 2018; Romberg et al. 2013), accelerating rotarod(Yoshioka et al. 2017), and acoustic startle response(Yoshioka et al. 2017). We also performed an elevated zero maze assessment of anxiety-like behaviors as a control experiment, and the tail-suspension test. (Altered performance on the tail suspension test is associated with lithium treatment(O'Donnell and Gould 2007), which we deemed relevant as BPNT2 is a direct inhibitory target of lithium.) However, we did not observe statistically significant alterations in behavioral performance between *Bpnt2*$^{fl/fl}$ and *Bpnt2*$^{fl/fl}$ Nestin-Cre mice on any of the assays performed (Figures 4A–4G).

Discussion

BPNT2 is an enzyme that breaks down the by-product of glycosaminoglycan sulfation reactions. Loss of BPNT2 impairs chondroitin-4-sulfation, which is an important component of the extracellular matrix across a variety of tissues. BPNT2 is also an inhibitory target of lithium, which is a widely prescribed mood stabilizer (Cade 1949) used to treat bipolar disorder, which motivates us to investigate the function of BPNT2 specifically in the brain. In this work, we report the generation of a nervous system-specific *Bpnt2*-knockout mouse, which is viable and does not portray obvious phenotypic aberrations. This is in contrast to our previous reports of severe skeletal defects in the germline *Bpnt2*-knockout mouse, which lead to perinatal lethality (Frederick et al. 2008), presumably due to pulmonary insufficiency. We now report that absence of functional BPNT2 in the nervous system does not result in lethality, and was not the cause of lethality in the germline knockout mouse.

Global knockout of BPNT2 impairs total-body chondroitin sulfation (Frederick et al. 2008). The effect of this impairment in cartilage is abnormal long bone development (chondrodysplasia) (Frederick et al. 2008; Nizon et al. 2012; Vissers et al. 2011), which can be observed in the human disorder characterized by homozygous BPNT2 mutations. To our knowledge, in-depth studies of the neurocognitive profiles of human patients with homozygous *BPNT2* mutations have not been reported, but there is reason to suspect that brain function could be affected. Of the six published cases of homozygous *BPNT2* mutation in humans, one patient was noted to have intellectual disability (Nizon et al. 2012).

Because chondroitin sulfate is an abundant glycosaminoglycan in the central nervous system, we sought to determine whether the loss of BPNT2 specifically in the nervous system would alter chondroitin sulfate biology in the brain. Analysis of brain tissue from *Bpnt2*$^{fl/fl}$ Nestin-Cre mice indeed demonstrated diminished chondroitin-4-sulfation, which corresponded to an increase in unsulfated chondroitin, as expected. However, we also identified a correspondent increase in chondroitin-6-sulfate. While such an increase was not identified in the cartilage of somatic *Bpnt2*-knockout mice, we did observe this increase in fibroblast cell lines taken from the *Bpnt2*-knockout mouse (Eisele et al. 2021). Chondroitin-6-sulfate is the next most abundant form of chondroitin sulfate after chondroitin-4-sulfate, and the two have been show to have opposing roles in regulating synaptic plasticity (Miyata et al. 2012). Chondroitin-6-sulfate promotes plasticity and is the predominant species in the brain in early life, while chondroitin-4-sulfate inhibits plasticity and is more abundant in adult brain (Miyata et al. 2012).

What is especially noteworthy about our observed increase in chondroitin-6-sulfate in the brains of our experimental animals is that changes in chondroitin-6-sulfate have been identified in the brains of human patients with bipolar disorder (H. Pantazopoulos et al. 2015). Specifically, decreases in chondroitin-6-sulfate were identified in patients with bipolar disorder relative to healthy controls, and exposure to lithium appeared to have a corrective effect; that is, lithium was associated with an increase in chondroitin-6-sulfate, as measured by immunohistochemistry (H. Pantazopoulos et al. 2015). We now report that the loss of a lithium-inhibited enzyme increases chondroitin-6-sulfation in the brain. Because we have previously shown that alterations in sulfation seen with *Bpnt2*-knockout stem from a loss of the enzyme's catalytic activity, we postulate that lithium-mediated inhibition of BPNT2 could underlie the effects on chondroitin-6-sulfate seen with lithium treatment of human patients.

Given the biochemical alteration of the chondroitin sulfation profile seen in brain tissue from *Bpnt2*$^{fl/fl}$ Nestin-Cre mice, it is interesting that we did not observe differences in PNN histology. Previous work has analyzed the consequences of nervous system-specific deletion of the proteoglycan core protein aggrecan, which plays a critical role in glycosaminoglycan biology (Rowlands et al. 2018). Somatic homozygous mutations in aggrecan cause skeletal malformations as well as perinatal lethality (Watanabe et al. 1994), very similar to what is seen with homozygous *Bpnt2*-knockout. Nervous system-specific deletion of aggrecan (using the Nestin-Cre driver) completely abolishes WFA staining in the brain (Rowlands et al. 2018). When undertaking the studies presented in this work, we considered it possible that we would observe a similarly dramatic effect in a nervous system-specific

Bpnt2 knockout. The somatic deletion of another gene relevant for chondroitin synthesis (CSGalNacT1, an enzyme critical for sugar chain synthesis), results in milder skeletal abnormalities, but still produces measurable disruption of WFA staining in brain tissue as well as behavioral anomalies (Yoshioka et al. 2017). The absence of such changes in a nervous system-specific *Bpnt2* knockout mouse is therefore an unexpected finding that could indicate a unique role of the BPNT2 enzyme. We can measure significant alterations in cerebral chondroitin sulfation that coincide with loss of BPNT2, but these are not so severe as to result in concomitant alterations in the PNN number or intensity. Nevertheless, chondroitin-sulfates (especially chondroitin-4-sulfate) are one of the major components of adult PNNs (Miyata and Kitagawa 2016b); where, then, is the loss of chondroitin-4-sulfate occurring?

Not all chondroitin-4-sulfate in the brain is localized to the WFA-reactive perineuronal nets themselves. Much of the chondroitin-4-sulfate in the brain is present in the loose extracellular matrix, which is not aggregated around specific cells. It could be that this loose matrix, which does not have as robust of a marker as condensed, pericellular PNNs do, is where the decrease in chondroitin-4-sulfate is physiologically relevant. To again contrast BPNT2 with other proteins that are important for chondroitin biology, the loss of aggrecan and CSGalNacT1 would be expected to affect the chondroitin species regardless of their locus of sulfation. However, this work and our prior work (Eisele et al. 2021b) suggest that of the three predominant species of chondroitin-sulfate, only chondroitin-4-sulfate is decreased with loss of BPNT2, while the ratios of chondroitin-6-sulfate and unsulfated chondroitin to total chondroitin are both elevated. While the increase in unsulfated chondroitin is to be expected, the increase in chondroitin-6-sulfate could be an attempt at a compensatory response. As WFA does not stain a specific sulfation moiety, this could explain why we did not observe alterations in WFA staining. There is also some work which suggests that the WFA-reactive, condensed PNNs are richer in chondroitin-6-sulfate and unsulfated chondroitin than the loose extracellular matrix is (Deepa et al. 2006), despite the major component of condensed PNNs still being chondroitin-4-sulfate. It may be that the degree of decrease in chondroitin-4-sulfate, coupled with the correspondent increase in chondroitin-6-sulfate, is not sufficient to alter PNNs histologically.

The lack of apparent alteration in PNNs could, in part, explain why we did not observe behavioral alterations in *Bpnt2*$^{fl/fl}$ Nestin-Cre mice. If the PNNs are robust to the changes we observed in chondroitin-4-sulfate, then we would expect them to function normally, and behaviors associated with PNNs would be unchanged in the absence of BPNT2. However, the selection of behavioral assays used in this work is by no means exhaustive. One analytical metric that is strongly associated with PNNs is ocular dominance plasticity, which is the ability to shift which eye is dominant by occluding vision in the dominant eye. This propensity for plasticity is typically present in juvenile animals, but not adults. Disruption of PNNs is associated with renewed ocular dominance plasticity, even after the closure of the juvenile critical period(Pizzorusso et al. 2002; Rowlands et al. 2018). Future studies may investigate whether *Bpnt2*$^{fl/fl}$ Nestin-Cre animals display differences in assessments of ocular dominance plasticity, given their altered chondroitin sulfation profile.

Acknowledgements:

We acknowledge the Knockout Mouse Project (KOMP) at the University of California-Davis for supplying Tm1a animals which were the precursors to all animal experiments described herein. The authors would like to thank Ryan Irving, Garrett Kaas, and Jane Wright for technical guidance and advice; the Vanderbilt University Medical Center Translational Pathology Shared Resource (supported by NCI/NIH Cancer Center Support Grant 5P30 CA68485-19) for help with tissue processing; the Bruce Carter lab for assistance with fluorescent microscopy; and John Allison, Fiona Harrison, and Krista Paffenroth of the Vanderbilt Mouse Neurobehavioral Lab for assistance with behavioral assays.

Funding:

This work was supported by funds from Vanderbilt University School of Medicine and the Natalie Overall Warren Professorship [to JDY] and the National Institutes of Health [T32GM007347 to BSE]. The content is solely the responsibility of the authors and does not necessarily represent the official views of the National Institutes of Health.

Abbreviations:

(BPNT2)	bisphosphate nucleotidase 2
(PAP)	phosphoadenosine phosphate
(AMP)	adenosine monophosphate
(PNN)	perineuronal net
(C4S)	chondroitin-4-sulfate
(C6S)	chondroitin-6-sulfate
(C0S)	unsulfated chondroitin
(GAG)	glycosaminoglycan
WFA	(*Wisteria floribunda* agglutinin)

References

Baker Kathryn D., Gray Arielle R., and Richardson Rick. 2017. “The Development of Perineuronal Nets around Parvalbumin Gabaergic Neurons in the Medial Prefrontal Cortex and Basolateral Amygdala of Rats.” Behavioral Neuroscience 131 (4): 289–303. 10.1037/bne0000203. [PubMed: 28714715]

Benard V, Vaiva G, Masson M, and Geoffroy PA. 2016. “Lithium and Suicide Prevention in Bipolar Disorder.” L’Encephale 42 (3): 234–41. 10.1016/j.encep.2016.02.006.

Benes Francine M., and Berretta Sabina. 2001. “GABAergic Interneurons: Implications for Understanding Schizophrenia and Bipolar Disorder.” Neuropsychopharmacology 25 (1): 1–27. 10.1016/S0893-133X(01)00225-1. [PubMed: 11377916]

Berretta Sabina, Pantazopoulos Harry, Markota Matej, Brown Christopher, and Batzianouli Eleni T.. 2015. “Losing the Sugar Coating: Potential Impact of Perineuronal Net Abnormalities on Interneurons in Schizophrenia.” Schizophrenia Research 167 (1–3): 18–27. 10.1016/j.schres.2014.12.040. [PubMed: 25601362]

Brückner G, and Grosche J. 2001. “Perineuronal Nets Show Intrinsic Patterns of Extracellular Matrix Differentiation in Organotypic Slice Cultures.” Experimental Brain Research 137 (1): 83–93. [PubMed: 11310175]

Cade JFJ 1949. “Lithium Salts in the Treatment of Psychotic Excitement.” The Medical Journal of Australia 2 (10): 349–52. 10.1080/j.1440-1614.1999.06241.x. [PubMed: 18142718]

Deepa Sarama Sathyaseelan, Carulli Daniela, Galtrey Clare, Rhodes Kate, Fukuda Junko, Mikami Tadahisa, Sugahara Kazuyuki, and Fawcett James W.. 2006. “Composition of Perineuronal Net Extracellular Matrix in Rat Brain: A Different Disaccharide Composition for the Net-Associated Proteoglycans.” The Journal of Biological Chemistry 281 (26): 17789–800. 10.1074/jbc.M600544200. [PubMed: 16644727]

Donegan Jennifer J, and Lodge Daniel J. 2016. “Hippocampal Perineuronal Nets Are Required for the Sustained Antidepressant Effect of Ketamine.” International Journal of Neuropsychopharmacology 20 (4): 354–58. 10.1093/ijnp/pyw095.

Dzyubenko Egor, Gottschling Christine, and Faissner Andreas. 2016. “Neuron-Glia Interactions in Neural Plasticity: Contributions of Neural Extracellular Matrix and Perineuronal Nets.” Neural Plasticity 2016. 10.1155/2016/5214961.

Eisele Brynna S., Luka Zigmund, Wu Alice J., Yang Fei, Hale Andrew T., and York John D.. 2021. “Sulfation of Glycosaminoglycans Depends on Catalytic Activity of Lithium-Inhibited Phosphatase BPNT2 in Vitro.” Journal of Biological Chemistry 0 (0). 10.1016/j.jbc.2021.101293.

Farndale Richard W., Buttle David J., and Barrett Alan J.. 1986. “Improved Quantitation and Discrimination of Sulphated Glycosaminoglycans by Use of Dimethylmethylene Blue.” Biochimica et Biophysica Acta (BBA) - General Subjects 883 (2): 173–77. 10.1016/0304-4165(86)90306-5. [PubMed: 3091074]

Forlenza OV, De-Paula VJR, and Diniz BSO. 2014. “Neuroprotective Effects of Lithium: Implications for the Treatment of Alzheimer’s Disease and Related Neurodegenerative Disorders.” ACS Chemical Neuroscience 5 (6): 443–50. 10.1021/cn5000309. [PubMed: 24766396]

Frederick Joshua P., Tafari A. Tsahai, Wu Sheue-Mei, Megosh Louis C., Chiou Shean-Tai, Irving Ryan P., and York John D.. 2008. “A Role for a Lithium-Inhibited Golgi Nucleotidase in Skeletal Development and Sulfation.” Proceedings of the National Academy of Sciences of the United States of America 105 (33): 11605–12. 10.1073/pnas.0801182105. [PubMed: 18695242]

Fukuda Minoru, Hiraoka Nobuyoshi, Akama Tomoya O., and Fukuda Michiko N.. n.d. “Carbohydrate-Modifying Sulfotransferases: Structure, Function, and Pathophysiology.” Journal of Biological Chemistry. Accessed November 14, 2019. 10.1074/jbc.R100049200.

Gogolla Nadine, Caroni Pico, Lüthi Andreas, and Herry Cyril. 2009. “Perineuronal Nets Protect Fear Memories from Erasure.” Science 325 (5945): 1258–61. 10.1126/science.1174146. [PubMed: 19729657]

Hudson Benjamin H., and York John D.. 2012. “Roles for Nucleotide Phosphatases in Sulfate Assimilation and Skeletal Disease.” Advances in Biological Regulation 52 (1). 10.1016/j.advenzreg.2011.11.002.

Karimi Atieh, Bahrampour Kobra, Moghaddam Mohammad Amin Momeni, Asadikaram Gholamreza, Ebrahimi Ghasem, Torkzadeh-Mahani Masoud, Tarzi Mojdeh Esmaeili, and Nematollahi Mohammad Hadi. 2017. “Evaluation of Lithium Serum Level in Multiple Sclerosis Patients: A Neuroprotective Element.” Multiple Sclerosis and Related Disorders 17 (October): 244–48. 10.1016/j.msard.2017.08.019. [PubMed: 29055468]

Lasek Amy W., Chen Hu, and Chen Wei-Yang. 2017. “Releasing Addiction Memories Trapped in Perineuronal Nets.” Trends in Genetics, December. 10.1016/j.tig.2017.12.004.

Lord Samuel J., Velle Katrina B., Mullins R. Dyche, and Fritz-Laylin Lillian K.. 2020. “SuperPlots: Communicating Reproducibility and Variability in Cell Biology.” Journal of Cell Biology 219 (6). 10.1083/jcb.202001064.

Mauney Sarah A., Athanas Katina M., Pantazopoulos Harry, Shaskan Noel, Passeri Eleonora, Berretta Sabina, and Woo Tsung-Ung W.. 2013. “Developmental Pattern of Perineuronal Nets in the Human Prefrontal Cortex and Their Deficit in Schizophrenia.” Biological Psychiatry 74 (6): 427–35. 10.1016/j.biopsych.2013.05.007. [PubMed: 23790226]

Mitchell Kevin J., Pinson Kathy I., Kelly Olivia G., Brennan Jane, Zupicich Joel, Scherz Paul, Leighton Philip A., et al. 2001. “Functional Analysis of Secreted and Transmembrane Proteins Critical to Mouse Development.” Nature Genetics 28 (3): 241–49. 10.1038/90074. [PubMed: 11431694]

Miyata Shinji, and Kitagawa Hiroshi. 2016a. “Chondroitin 6-Sulfation Regulates Perineuronal Net Formation by Controlling the Stability of Aggrecan.” Neural Plasticity 2016: 1305801. 10.1155/2016/1305801. [PubMed: 27057358]

———. 2016b. “Chondroitin Sulfate and Neuronal Disorders.” Frontiers in Bioscience (Landmark Edition) 21: 1330–40. [PubMed: 27100510]

Miyata Shinji, Komatsu Yukio, Yoshimura Yumiko, Taya Choji, and Kitagawa Hiroshi. 2012. “Persistent Cortical Plasticity by Upregulation of Chondroitin 6-Sulfation.” Nature Neuroscience 15 (3): 414–22, S1–2. 10.1038/nn.3023. [PubMed: 22246436]

“Neuroprotective Effects of Lithium in Patients with Bipolar.” n.d. Accessed February 1, 2019. http://www.currentpsychopharmacology.com/articles/137888/neuroprotective-effects-of-lithium-in-patients-with-bipolar-disorder.

Nizon Mathilde, Alanay Yasemin, Tuysuz Beyhan, Kiper Pelin Ozlem Simsek, Geneviève David, Sillence David, Huber Celine, Munnich Arnold, and Cormier-Daire Valérie. 2012. “IMPAD1 Mutations in Two Catel-Manzke like Patients.” American Journal of Medical Genetics. Part A 158A (9): 2183–87. 10.1002/ajmg.a.35504. [PubMed: 22887726]

O’Donnell Kelley C., and Gould Todd D.. 2007. “The Behavioral Actions of Lithium in Rodent Models.” Neuroscience and Biobehavioral Reviews 31 (6): 932–62. 10.1016/j.neubiorev.2007.04.002. [PubMed: 17532044]

Pantazopoulos H, Markota M, Jaquet F, Ghosh D, Wallin A, Santos A, Caterson B, and Berretta S. 2015. “Aggrecan and Chondroitin-6-Sulfate Abnormalities in Schizophrenia and Bipolar Disorder: A Postmortem Study on the Amygdala.” Translational Psychiatry 5 (1): e496. 10.1038/tp.2014.128. [PubMed: 25603412]

Pantazopoulos Harry, and Berretta Sabina. 2016. “In Sickness and in Health: Perineuronal Nets and Synaptic Plasticity in Psychiatric Disorders.” Research article. Neural Plasticity. 2016. 10.1155/2016/9847696.

Pantazopoulos Harry, Woo Tsung-Ung W., Lim Maribel P., Lange Nicholas, and Berretta Sabina. 2010. “Extracellular Matrix-Glial Abnormalities in the Amygdala and Entorhinal Cortex of Subjects Diagnosed with Schizophrenia.” Archives of General Psychiatry 67 (2): 155–66. 10.1001/archgenpsychiatry.2009.196. [PubMed: 20124115]

Pizzorusso Tommaso, Medini Paolo, Berardi Nicoletta, Chierzi Sabrina, Fawcett James W., and Maffei Lamberto. 2002. “Reactivation of Ocular Dominance Plasticity in the Adult Visual Cortex.” Science 298 (5596): 1248–51. 10.1126/science.1072699. [PubMed: 12424383]

Romberg Carola, Yang Sujeong, Melani Riccardo, Andrews Melissa R., Horner Alexa E., Spillantini Maria G., Bussey Timothy J., Fawcett James W., Pizzorusso Tommaso, and Saksida Lisa M.. 2013. “Depletion of Perineuronal Nets Enhances Recognition Memory and Long-Term Depression in the Perirhinal Cortex.” Journal of Neuroscience 33 (16): 7057–65. 10.1523/JNEUROSCI.6267-11.2013. [PubMed: 23595763]

Rowlands Daire, Lensjø Kristian K., Dinh Tovy, Yang Sujeong, Andrews Melissa R., Hafting Torkel, Fyhn Marianne, Fawcett James W., and Dick Gunnar. 2018. “Aggrecan Directs Extracellular Matrix-Mediated Neuronal Plasticity.” Journal of Neuroscience 38 (47): 10102–13. 10.1523/JNEUROSCI.1122-18.2018. [PubMed: 30282728]

Saccà Francesco, Puorro Giorgia, Brunetti Arturo, Capasso Giovambattista, Cervo Amedeo, Cocozza Sirio, Leva Mariafulvia de, et al. 2015. “A Randomized Controlled Pilot Trial of Lithium in Spinocerebellar Ataxia Type 2.” Journal of Neurology 262 (1): 149–53. 10.1007/s00415-014-7551-0. [PubMed: 25346067]

Slaker Megan L., Harkness John H., and Sorg Barbara A.. 2016. “A Standardized and Automated Method of Perineuronal Net Analysis Using Wisteria Floribunda Agglutinin Staining Intensity.” IBRO Reports 1 (December): 54–60. 10.1016/j.ibror.2016.10.001. [PubMed: 28713865]

Sohaskey Michael L., Yu Jane, Diaz Michael A., Plaas Anna H., and Harland Richard M.. 2008. “JAWS Coordinates Chondrogenesis and Synovial Joint Positioning.” Development (Cambridge, England) 135 (13): 2215–20. 10.1242/dev.019950.

Sorg Barbara A., Berretta Sabina, Blacktop Jordan M., Fawcett James W., Kitagawa Hiroshi, Kwok Jessica C. F., and Miquel Marta. 2016. “Casting a Wide Net: Role of Perineuronal Nets in Neural Plasticity.” Journal of Neuroscience 36 (45): 11459–68. 10.1523/JNEUROSCI.2351-16.2016. [PubMed: 27911749]

Spijker Heleen M. van ‘t, and Kwok Jessica C. F.. 2017. “A Sweet Talk: The Molecular Systems of Perineuronal Nets in Controlling Neuronal Communication.” Frontiers in Integrative Neuroscience 11 (December). 10.3389/fnint.2017.00033.

Thompson Elise Holter, Kristian Kinden Lensjø Mattis Brænne Wigestrand, Anders Malthe-Sørenssen Torkel Hafting, and Fyhn Marianne. 2018. “Removal of Perineuronal Nets Disrupts Recall of a Remote Fear Memory.” Proceedings of the National Academy of Sciences of the United States of America 115 (3): 607–12. 10.1073/pnas.1713530115. [PubMed: 29279411]

Ueno Hiroshi, Takao Keizo, Suemitsu Shunsuke, Murakami Shinji, Kitamura Naoya, Wani Kenta, Okamoto Motoi, Aoki Shozo, and Ishihara Takeshi. 2018. “Age-Dependent and Region-Specific Alteration of Parvalbumin Neurons and Perineuronal Nets in the Mouse Cerebral Cortex.” Neurochemistry International 112 (January): 59–70. 10.1016/j.neuint.2017.11.001. [PubMed: 29126935]

Vissers Lisenka E. L. M., Lausch Ekkehart, Unger Sheila, Ana Belinda Campos-Xavier Christian Gilissen, Rossi Antonio, Del Rosario Marisol, et al. 2011. “Chondrodysplasia and Abnormal Joint Development Associated with Mutations in IMPAD1, Encoding the Golgi-Resident Nucleotide Phosphatase, GPAPP.” American Journal of Human Genetics 88 (5): 608–15. 10.1016/j.ajhg.2011.04.002. [PubMed: 21549340]

Watanabe H, Kimata K, Line S, Strong D, Gao LY, Kozak CA, and Yamada Y. 1994. “Mouse Cartilage Matrix Deficiency (Cmd) Caused by a 7 Bp Deletion in the Aggrecan Gene.” Nature Genetics 7 (2): 154–57. 10.1038/ng0694-154. [PubMed: 7920633]

Yang ML, Li JJ, So KF, Chen JYH, Cheng WS, Wu J, Wang ZM, Gao F, and Young W. 2012. “Efficacy and Safety of Lithium Carbonate Treatment of Chronic Spinal Cord Injuries: A Double-Blind, Randomized, Placebo-Controlled Clinical Trial.” Spinal Cord 50 (2): 141–46. 10.1038/sc.2011.126. [PubMed: 22105463]

Yoshioka Nozomu, Miyata Shinji, Tamada Atsushi, Watanabe Yumi, Kawasaki Asami, Kitagawa Hiroshi, Takao Keizo, Miyakawa Tsuyoshi, Takeuchi Kosei, and Igarashi Michihiro. 2017. “Abnormalities in Perineuronal Nets and Behavior in Mice Lacking CSGalNAcT1, a Key Enzyme in Chondroitin Sulfate Synthesis.” Molecular Brain 10 (October). 10.1186/s13041-017-0328-5.

Zheng C, and Levenston ME. 2015. “Fact versus Artifact: Avoiding Erroneous Estimates of Sulfated Glycosaminoglycan Content Using the Dimethylmethylene Blue Colorimetric Assay for Tissue-Engineered Constructs.” European Cells & Materials 29 (April): 224–36. [PubMed: 25890595]

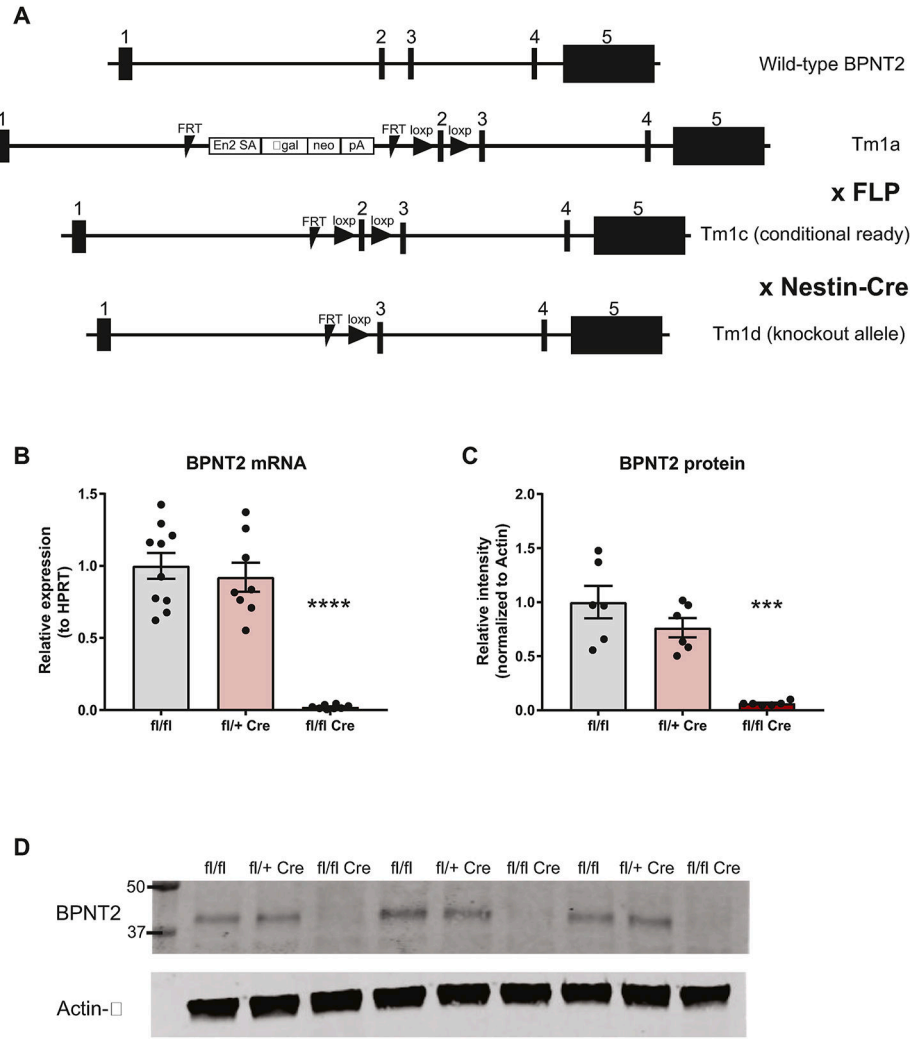

Figure 1. Generation of conditional and nervous system-specific *Bpnt2*-knockout mouse.

A. Schematic of knockout strategy. Tm1a mice obtained from UC-Davis KOMP and bred with FLPo-10 mice (Jackson #011065) to generate Tm1c (floxed) mice, which were then crossed with Nestin-Cre mice (Jackson #003771) to yield knockout (Tm1d allele) in nervous system tissues (neurons and astrocytes). B. mRNA expression of *Bpnt2* in cortical brain tissue. C. Quantification of protein expression from western blot and D. Western blot showing BPNT2 protein expression in cortical brain tissue. P-values are results of one-way ANOVA: ***p<0.001, ****p<0.0001.

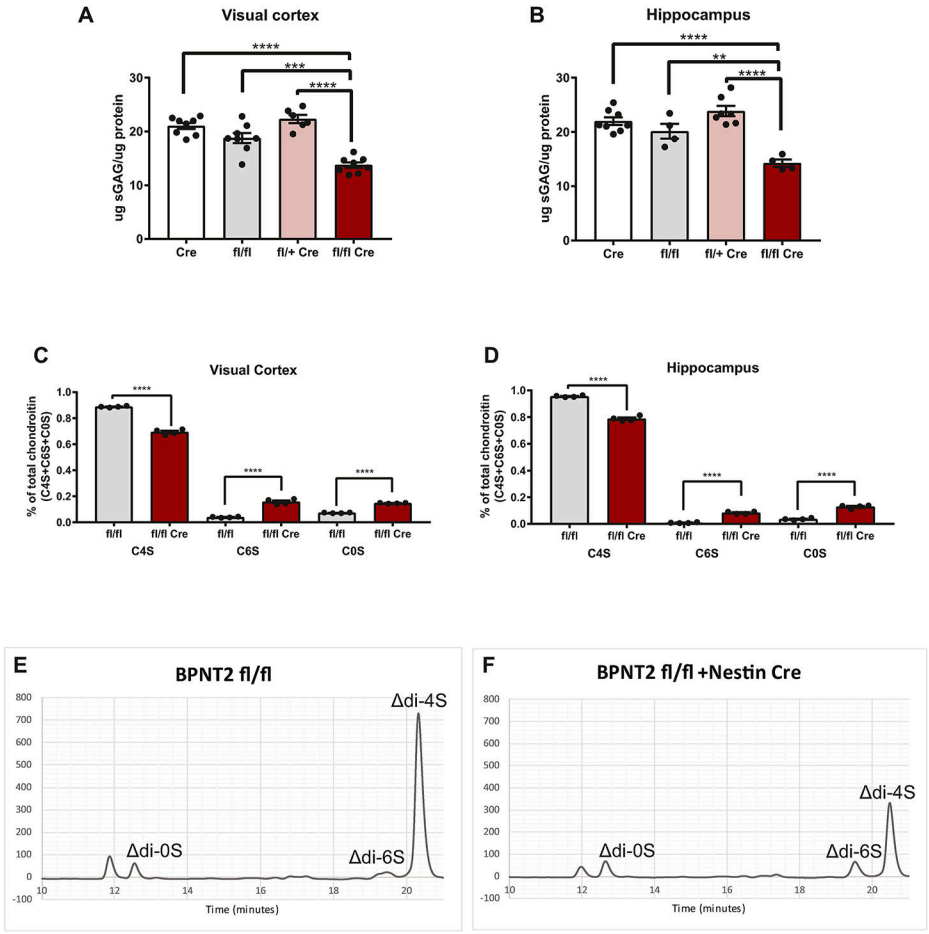

Figure 2. *Bpnt2*$^{fl/fl}$ Nestin-Cre mice exhibit altered glycosaminoglycan sulfation in brain tissues. Quantification of total GAG sulfation in A. visual cortex tissue and B. hippocampal tissue using DMMB assay. C. Quantification of chondroitin sulfate disaccharides in visual cortex tissue as measured by HPLC. D. Quantification of chondroitin sulfate disaccharides in hippocampal tissue as measured by HPLC. E. and F. Representative HPLC traces from chondroitin disaccharide HPLC performed on cortical tissue. Δdi-0S: unsulfated chondroitin disaccharide, Δdi-6S: chondroitin-6-sulfate disaccharide, Δdi-4S: chondroitin-4-sulfate disaccharide. P-values denote results of Tukey's post-hoc analyses following significant one-way ANOVA. **p<0.01, ***p<0.001, ****p<0.0001.

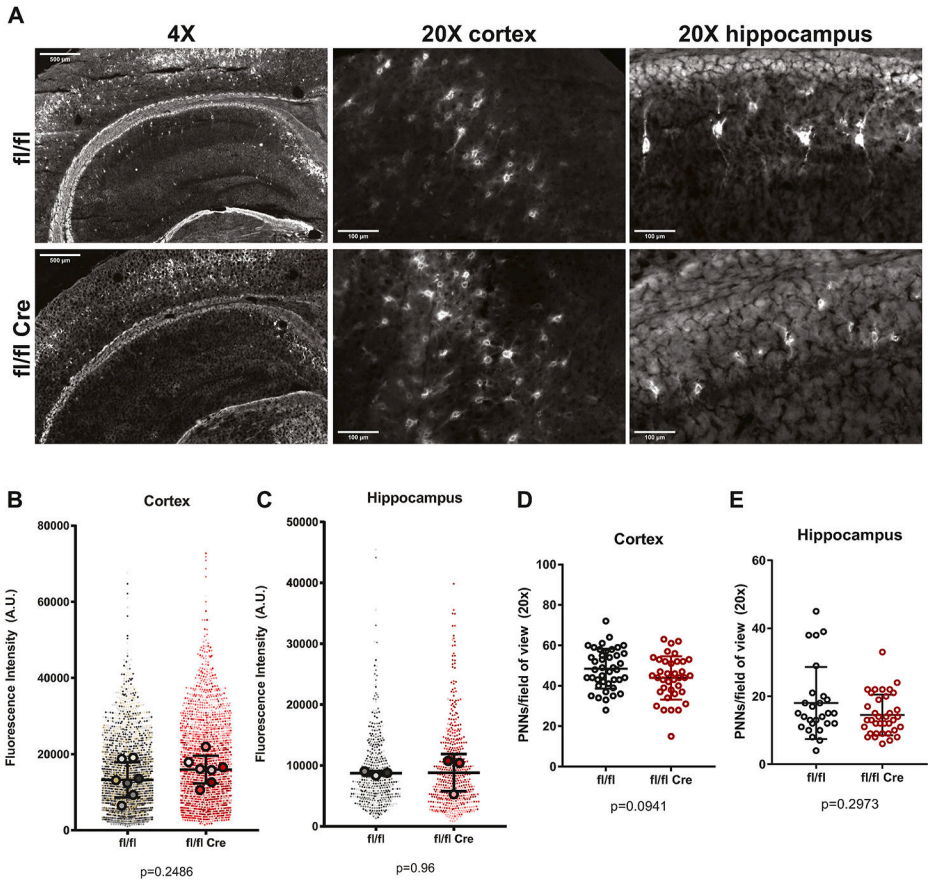

Figure 3. *Bpnt2*$^{fl/fl}$ Nestin-Cre mice do not exhibit gross alterations in perineuronal net staining.

A. Representative PNN staining from *Bpnt2*$^{fl/fl}$ and *Bpnt2*$^{fl/fl}$ Nestin-Cre animals. Quantification of perineuronal net intensity from tissue sections from B. cortical and C. hippocampal brain regions using Pipsqueak AI. D. and E. Analysis of number of PNNs detected per tissue section using Pipsqueak AI software. For B/C, p-values indicate results of two-sided student's t-test. For D/E, p-values indicate results of Mann-Whitney U-test.

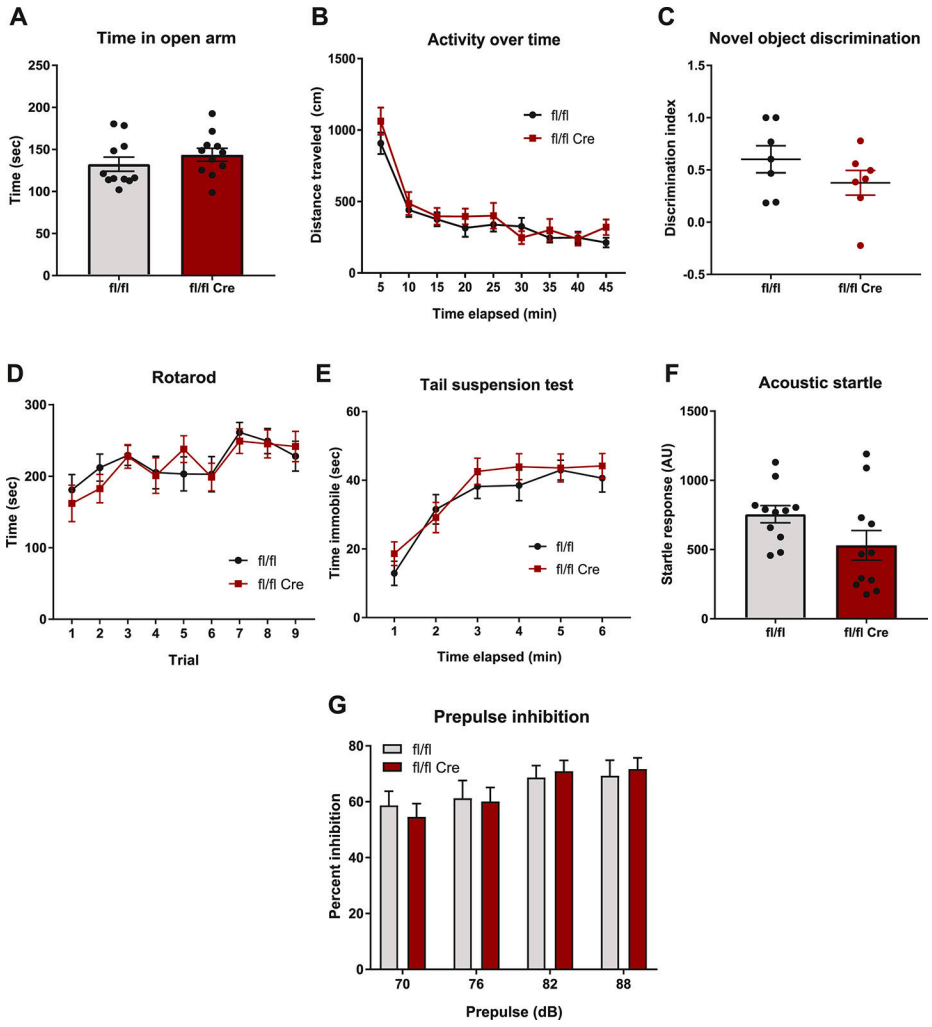

Figure 4. *Bpnt2*$^{fl/fl}$ Nestin-Cre mice do not exhibit gross abnormalities on key behavioral assays.
A. Elevated zero maze. B. Open field activity assessment, performed over 45 minutes. C. Novel object recognition. D. Accelerating rotarod motor learning assay. E. Tail suspension test. F. Acoustic startle. G. Prepulse inhibition.